MIND THE UNCERTAINTY: GLOBAL PLATE MODEL CHOICE IMPACTS DEEP-TIME PALAEOBIOLOGICAL STUDIES

Lucas Buffan[1,2*], Lewis A. Jones[1*], Mathew Domeier[3], Christopher R. Scotese[4], Sabin Zahirovic[5], and Sara Varela[1]

[1]Centro de Investigación Mariña, Grupo de Ecoloxía Animal, Universidade de Vigo, 36310 Vigo, Spain

[2]Département de Biologie, École Normale Supérieure de Lyon, Université Claude Bernard Lyon 1, 69342 Lyon Cedex 07, France

[3]Centre for Earth Evolution and Dynamics (CEED), University of Oslo, NO-0316 Oslo, Norway

[4]Department of Earth and Planetary Sciences, Northwestern University, Evanston, Illinois 60208, USA

[5]EarthByte Group, School of Geosciences, University of Sydney, Sydney, NSW 2006, Australia

*These authors contributed equally to this work

Corresponding authors:

Lucas Buffan (Lucas.L.Buffan@gmail.com) and Lewis A. Jones (LewisAlan.Jones@uvigo.es)

Running headline: Palaeogeographic Uncertainty in Palaeobiology

Keywords: Coral reefs, Crocodiles, Global Plate Models, Macroecology, Palaeobiogeography, Palaeobiology, Palaeoclimate, Palaeogeography, Phanerozoic

Abstract

1. Global Plate Models (GPMs) aim to reconstruct the tectonic evolution of the Earth by modelling the motion of the plates and continents through time. These models enable palaeobiologists to study the past distribution of extinct organisms. However, different GPMs exist that vary in their partitioning of the Earth's surface and the modelling of continental motions. Consequently, the preferred use of one GPM will influence palaeogeographic reconstruction of fossil occurrences and any inferred palaeobiological and palaeoclimatic conclusion.
2. Here, using five open-access GPMs, we reconstruct the palaeogeographic distribution of cell centroids from a global hexagonal grid and quantify palaeogeographic uncertainty across the entire Phanerozoic (540–0 Ma). We measure uncertainty between reconstructed coordinates using two metrics: (1) palaeolatitudinal standard deviation and (2) mean pairwise geodesic distance. Subsequently, we evaluate the impact of GPM choice on palaeoclimatic reconstructions when using fossil occurrence data. To do so, we use two climatically-sensitive entities (coral reefs and crocodylomorphs) to infer the palaeolatitudinal extent of subtropical climatic conditions for the last 240 million years.
3. Our results indicate that differences between GPMs increase with the age of reconstruction. Specifically, cell centroids rotated to older intervals show larger differences in palaeolatitude and geographic spread than those rotated to younger intervals. However, high palaeogeographic uncertainty is also observed in younger intervals within tectonically complex regions (i.e. in the vicinity of terrane and plate boundaries). We also show that when using fossil data to infer the distribution of subtropical climatic conditions across the last 240 Ma, estimates vary by 6–7° latitude on average, and up to 24° latitude in extreme cases.
4. Our findings confirm that GPM choice is an important consideration when studying past biogeographic patterns and palaeoclimatic trends. We recommend using GPMs that report true

palaeolatitudes (through palaeomagnetic data use) and incorporating palaeogeographic uncertainty into palaeobiological analyses.

Introduction

Akin to neontologists, palaeobiologists seek to understand the origin, distribution, and extinction of species across time and space (e.g. Alroy, 2014; Powell et al., 2015; Spano et al., 2016; Meseguer and Condamine, 2020; Boddy et al., 2022). However, while neontologists can study the present-day geographic distribution of taxa, palaeobiologists must contend with the shift of the continents over geological timescales. Specifically, the geographic location of fossil occurrences on the Earth's surface today does not necessarily represent their location *in vivo*; fossil remains found at tropical latitudes might have been deposited at temperate latitudes, and vice versa. Consequently, reconstructing the past geographic distribution–i.e. the palaeogeographic distribution–of fossil occurrences is fundamental to the study of macroecological patterns in deep time. To do so, palaeobiologists routinely use what are known as Global Plate Models (e.g. Brocklehurst et al., 2017; Allen et al., 2020; Dunne et al., 2020; Antell et al., 2020; Boddy et al., 2022; Jones et al., 2022; Zhang et al., 2022).

Global Plate Models (GPMs) aim to reconstruct the tectonic evolution of the Earth, modelling the motion of the continents across its surface through geological time. They do so using Euler's rotation theorem to describe the motion of geometries–such as tectonic plates or geological terranes–on a sphere (McKenzie and Parker, 1967; Morgan, 1968). Since the 1970s, numerous GPMs have been developed by both the scientific community (e.g. Scotese et al., 1988; Müller et al., 1993, 2019; Golonka et al., 1994; Golonka, 2007; Torsvik et al., 2008a; Seton et al., 2012; Domeier and Torsvik, 2014; Matthews et al., 2016; Torsvik and Cocks, 2017; Scotese and Wright, 2018; Vérard, 2019; Young et al., 2019; Merdith et al., 2021) and industry (e.g. Getech plc and Robertson Research) for purposes such as geological resource exploration (Markwick, 2019) and Earth System modelling (Lunt et al., 2016). A more recent shift to 'full-plate models' (e.g. Merdith et al., 2021) and deforming plate models (e.g. Gurnis et al., 2018; Müller et al., 2019) has increased the complexity of GPMs by describing–in detail–

how plate boundaries, deforming regions, and the plate-mantle system have evolved through time (Seton et al., 2023).

A GPM is made up of two key components. The first component is a set of 'geometries' dividing the surface of the Earth into individual tectonic elements that can be independently reconstructed. These elements include both 'dynamic polygons' (also known as 'continuously closing plate polygons'), which change shape through time, and 'static polygons', whose shape and size are fixed. The former are used to model entire tectonic plates, whereas the latter are used to delineate continents, fault-bound tectonic blocks ('terranes'), or any other arbitrary parcel of crust whose shape and size can be treated as fixed through the modelled time. Whether any given continent or crustal block can be appropriately treated as a static polygon depends on the spatial resolution and timescale being considered, and so the number and definition of static polygons can vary significantly between GPMs (with more recent and temporally more extensive GPMs tending to have more static polygons), resulting in differential partitioning of the Earth's surface (Fig. S1). Differences in the polygonization of the Earth's surface between GPMs also arise from different interpretations about the locations of ancient tectonic boundaries—which occurs more frequently in complicated geological areas and in deeper time.

The second key component of a GPM is a rotation file that describes the time-dependent motion of the tectonic elements as finite (or "total") Euler rotations (Müller et al., 2018; Domeier and Torsvik, 2019). These 'rotation files' can be read and interpolated by software programs such as 'GPlates' (Müller et al., 2018) to reconstruct the motion of the tectonic elements through time, and enable the reconstruction of palaeocoordinates for fossil occurrence data (Boyden et al., 2011; Wright et al., 2013). It is important to note that rotation files can report the motion of tectonic elements with respect to one another ('relative' motion) and/or with respect to the Earth's mantle *or* the planetary spin-axis (so-called 'absolute' motion) (Torsvik et al., 2008a). Only the latter reference frame (the motion of tectonic elements relative to Earth's spin axis) is appropriate for the reconstruction of fossil occurrence data as it reports true palaeolatitudes (Seton et al. 2023). Recent work has demonstrated differences in the

palaeogeographic reconstruction of several fossil and geological datasets when using different GPMs (e.g. Cao et al., 2019; Boddy et al., 2022; Jones et al., 2022). Yet, the impact of model choice on palaeogeographic reconstructions at global Phanerozoic scale remains untested.

Quantifying this 'palaeogeographic uncertainty' is key to understanding the robustness of observed deep-time biodiversity patterns and their response to past climatic change (e.g. Mannion et al., 2014; Reddin et al., 2018). Here, we quantify spatial discrepancies in palaeogeographic reconstruction from five open-access GPMs. To do so, we reconstruct the palaeogeographic coordinates (i.e. palaeocoordinates) of centroids from a global hexagonal grid (~100 km spacing) across the last 540 million years (Myr). By comparing these five reconstructions, we identify key spatial zones and timeframes of palaeogeographic uncertainty. Subsequently, we reconstruct the palaeogeographic distribution of two climatically-sensitive entities (fossil coral reefs and terrestrial crocodylomorphs) to evaluate the impact of GPM choice on estimations of the palaeolatitudinal extent of tropical climatic conditions over the last 240 Myr. We hypothesise that: (1) differences in palaeogeographic reconstruction increase with age, and (2) GPM choice can significantly influence reconstructions of palaeogeographic distributions of organisms and inferred palaeoclimatic conditions.

Materials and Methods

Global Plate Models

Five open-access Global Plate Models (GPMs) were used to evaluate spatiotemporal differences in palaeogeographic reconstructions: WR13 (Wright et al., 2013), MA16 (Matthews et al., 2016), TC17 (Torsvik and Cocks, 2017), SC16 (Scotese, 2016; Scotese and Wright, 2018), and ME21 (Merdith et al., 2021). These GPMs have variable temporal coverage (see Table 1) with WR13, SC16, TC17, and ME21 covering the entirety of our Phanerozoic study period (540–0 Ma), while MA16 is limited to the Devonian–Recent (410–0 Ma).

Table 1: A summary table of the Global Plate Models used in this study. The table includes the abbreviations used in this study, the names of models according to the GPlates Web Service (https://gwsdoc.gplates.org), the temporal coverage of each model, and the relevant reference for each model.

Abbreviation	GPlates ID	Temporal coverage	Reference
WR13	GOLONKA	0–550 Ma	(Wright et al., 2013)
MA16	MATTHEWS2016_pmag_ref	0–410 Ma	(Matthews et al., 2016)
TC17	TorsvikCocks2017	0–540 Ma	(Torsvik and Cocks, 2017)
SC16	PALEOMAP	0–1100 Ma	(Scotese, 2016; Scotese and Wright, 2018)
ME21	MERDITH2021	0–1000 Ma	(Merdith et al., 2021)

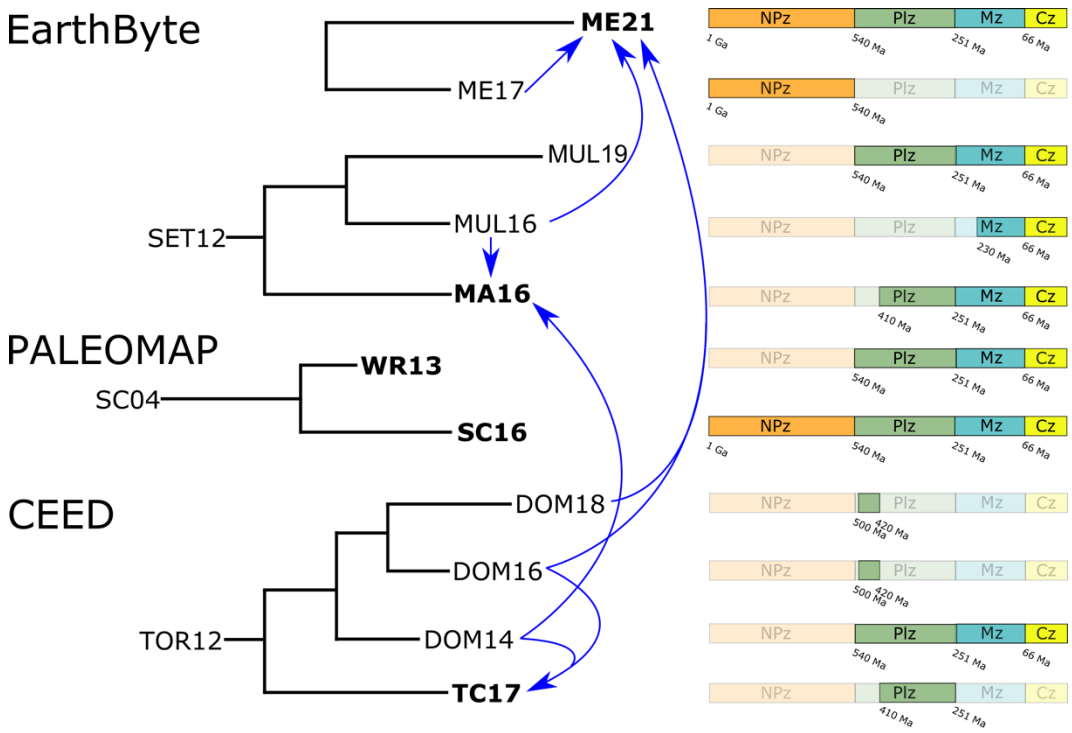

Figure 1: A 'cladogram'-type representation of the relationship between Global Plate Models from the three main model development groups (EarthByte, PALEOMAP project, and Centre for Earth Evolution and Dynamics (CEED)) used in this study, and their respective temporal coverage. Blue arrows indicate 'horizontal transfers' between models, i.e. amalgamations of models from different

groups. Global Plate Model abbreviations: TOR12 (Torsvik et al., 2012), DOM14 (Domeier and Torsvik, 2014), TC17 (Torsvik and Cocks, 2017), DOM16 (Domeier, 2016), DOM18 (Domeier, 2018), MA16 (Matthews et al., 2016), ME17 (Merdith et al., 2017), ME21 (Merdith et al., 2021), MUL16 (Müller et al., 2016), MUL19 (Müller et al., 2019), SC04 (Scotese, 2004), SC16 (Scotese, 2016; Scotese and Wright, 2018), SET12 (Seton et al., 2012), WR13 (Wright et al., 2013). Models included in this study are represented in bold. Era abbreviations: Cenozoic (Cz), Mesozoic (Mz), Palaeozoic (Plz), and Neo-Proterozoic (NPz).

WR13 and SC16 both share a common lineage stemming from the plate model of Scotese (2004), but WR13 employed modifications to fit palaeomagnetic data summarised in (Torsvik and Van der Voo, 2002), whereas SC16 was used to produce the widely-used set of Phanerozoic paleogeographic maps and digital elevation models (Scotese and Wright, 2018). The Scotese GPM has evolved slowly over the last three decades. Small, but significant, changes have occurred in the location of the core continents (e.g. North America, Europe, Gondwana), whereas major changes have occurred in the placement of N. China, S. China, Cimmeria, and the exotic terranes of western North America (Fig. S2). The time range of the Scotese GPM has also been extended further into the Precambrian (Scotese, 2004, 2016; Scotese and Elling, 2017). TC16 primarily stems from the global paleomagnetic model of Torsvik et al. (2012), but it incorporates some changes made in the subsequent plate models of Domeier and Torsvik (2014) for the late Palaeozoic (410–250 Ma), and Domeier (2016) in the earlier Palaeozoic (500–410 Ma). Note that TC16 is presented in a mantle reference frame by default, but here we use the version which is available in the paleomagnetic reference frame. The model of MA16 is likewise built upon the model of Domeier and Torsvik (2014) for the late Paleozoic (410–250), and so MA16 and TC16 are very similar for that interval of time. For Mesozoic and Cenozoic time, MA16 is based on the model of Müller et al. (2016). Note that the model of Müller et al. (2016) exists in a mantle reference frame, and so too does the original model of MA16 for times between 250 and 0 Ma. However, a version cast into the paleomagnetic reference frame was subsequently made available, using the global apparent

polar wander path from Torsvik et al. (2012), and here we utilize this later version. ME21 is largely a composition of several pre-existing models, namely the model of Merdith et al. (2017) from 1000–500 Ma, the models of Domeier (2016; 2018) for the early Palaeozoic (500–410 Ma), and a modified version of Young et al. (2019) for the interval 410–0 Ma, and the entire 1000–0 Ma model interval is cast into a paleomagnetic reference frame. The model of Young et al. (2019) is modified from Matthews et al. (2016), which again was built from Domeier and Torsvik (2014) for the late Palaeozoic interval (410–250 Ma) and Müller et al. (2016) from 230–0 Ma. Thus, for the Palaeozoic interval (particularly the late Palaeozoic), there is some common ancestry between TC16, MA16 and ME21, and this extends into the Mesozoic and Cenozoic for MA16 and ME21. Nevertheless, the modifications made between these alternative models is a reflection of outstanding paleogeographic uncertainty. Figure 1 summarises the main interrelationships between these various GPMs.

Quantifying spatiotemporal differences

To quantify differences in palaeogeographic reconstruction (Fig. 1), we first generated a discrete global hexagonal grid (~100 km spacings) via the python library 'h3' v.3.7.6 (Uber, 2023). Most GPMs have a network of static polygons covering most of the Earth's continental areas, and we retained only the grid cells that were included within a static polygon in each of the GPMs. Subsequently, we reconstructed palaeocoordinates for cell centroids across the last 540 Myr with a timestep of 10 Myr for each GPM, resulting in up to 54 time steps depending on GPM (Table 1). To do so, we used the python library 'pygplates' ver. 0.36.0 (Williams et al., 2017) to interact with the software GPlates (Boyden et al., 2011; Müller et al., 2018). Using the reconstructed palaeocoordinates for each cell–from each model–we calculated: (1) the standard deviation (SD) in palaeolatitude and (2) the mean pairwise geodesic distance (PGD) between reconstructed coordinates (up to five sets) for each cell. The former of these quantifies the potential uncertainty in palaeolatitude between models with significance for studies such as those focused on reconstructing the latitudinal biodiversity gradients in deep time (e.g. Allen et al., 2020; Song et al., 2020). The latter quantifies the uncertainty in palaeogeographic position

between models having significance for studies focused on themes such as reconstructing organisms' geographic range sizes (e.g. Antell et al., 2020). Mean PGD was calculated using the R package 'geosphere' ver. 1.5-18 (Hijmans et al., 2021).

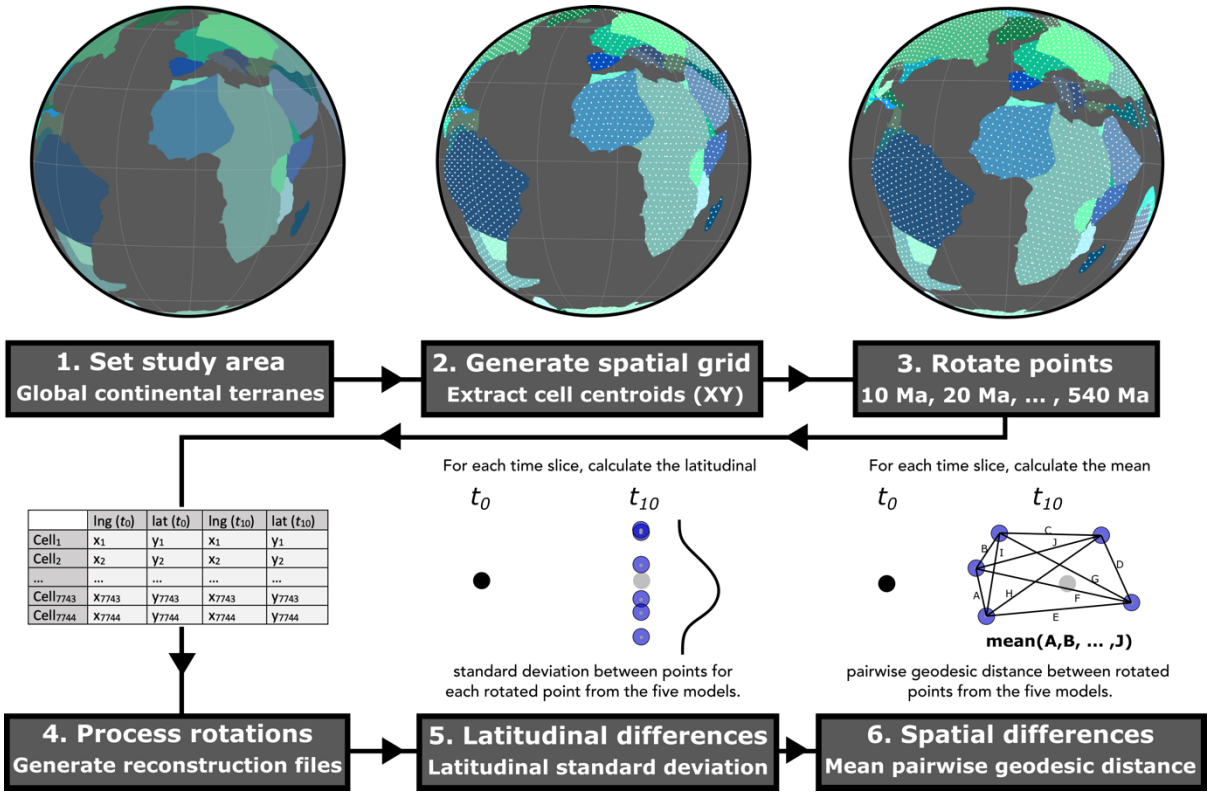

Figure 2: A graphical schematic of the simulation workflow used in this study. Using continental tectonic elements, the study area is first established (1). Subsequently, a discrete global hexagonal grid (~100 km spacings) is generated via the python library 'h3' v.3.7.6 (Uber, 2023) and cell centroids extracted for cells intersecting with the continental tectonic elements (2). Cell centroids are then rotated (3) at time intervals of 10 Myr throughout the Phanerozoic (540–0 Ma), for each model, using the software GPlates via the 'pygplates' ver. 0.36.0 python library (Williams et al., 2017). Reconstruction files are subsequently generated for each model (4), and the palaeolatitudinal standard deviation (5) and the mean pairwise geodesic distance (6) calculated for each cell centroid between the five models for each time step.

Palaeoclimatic reconstruction

To test the influence of GPM choice on fossil-based palaeoclimatic reconstructions, we estimate the palaeolatitudinal extent of (sub-)tropical climatic conditions using two climatically sensitive entities: warm-water coral reefs and terrestrial crocodylomorphs. These entities are frequently used to infer the extent of (sub-)tropical palaeoclimatic conditions due to their limited thermal tolerance and geographic distribution today (e.g. Markwick, 2007; Burgener et al., 2023). Fossil crocodylomorph occurrences (="Crocodylomorpha") were downloaded from The Paleobiology Database (https://paleobiodb.org/#/) on the 9th of November 2022 and were restricted to terrestrial taxa and body fossils. Marine taxa were excluded as they appear to be less constrained by climatic factors than terrestrial taxa (Mannion et al., 2015). Fossil coral reef occurrences were downloaded from the PaleoReef Database (Kiessling and Krause, 2022) on the 10th of March 2022 and were restricted to scleractinian 'true reefs' with a tropical affinity. This led us to exclude pre-Anisian reef occurrences. At the end of the cleaning, the midpoint age of oldest crocodylomorph occurrence was 232.5 Ma, and the oldest reef occurrence was 231.5 Ma. Finally, fossil occurrences were split into 10 Myr time bins using the midpoint age of each occurrence's age range. After data processing, 4638 terrestrial crocodylomorphs and 419 warm-water coral reef occurrences remained for analyses.

Using the five GPMs (Table 1), we reconstructed the palaeocoordinates for each occurrence based on the midpoint of its respective age range. Assuming hemispheric symmetry in climatic conditions, we subsequently identified the maximum absolute palaeolatitude within each time bin–for each model and entity–to infer the palaeolatitudinal extent of (sub-)tropical climatic conditions. Using this deduction, we quantified the potential uncertainty in the palaeolatitudinal extent of (sub-)tropical climatic conditions by calculating the palaeolatitudinal range between estimates for each time bin. Finally, for each fossil occurrence, we calculated the median, maximum and minimum reconstructed palaeolatitude from the five model estimates.

Results

Spatiotemporal discrepancy trends

Palaeolatitudinal SD and mean PGD demonstrate an increasing uncertainty in palaeogeographic reconstruction with age (Fig. 3–4; Fig. S3). Overall, GPMs are in good agreement for the last 100 Myr (mid-Cretaceous–Recent), with 97.4% of cells having a palaeolatitudinal SD less than 5º and a mean PGD less than 1000 km (Fig. 3). However, GPM reconstructions begin to substantially diverge at greater reconstruction ages with generally increasing uncertainty throughout the Mesozoic (251.9–66 Ma) and Palaeozoic (538.8–251.9 Ma). For example, in the Cenozoic (66–0 Ma), 1.9% of cells have a palaeolatitudinal SD of more than 5º, going up to 14.8% of cells during the Mesozoic, and 53.8% during the Palaeozoic (Fig. 3a). This trend is further reflected by an increase in mean PGD with 1.2% of cells having a value of more than 1000 km in the Cenozoic, 20.2% during the Mesozoic, and 80% during the Palaeozoic (Fig. 3b). Differences in Cambrian (538.8–485.4 Ma) reconstructions are especially large, with a considerable proportion of cells having a palaeolatitudinal SD of more than 5º (~76.3%) and mean PGD of more than 1000 km (~90.1%) (Fig. 3; Fig. S3). Notably, despite this overall trend of increasing palaeogeographic uncertainty with age, uncertainty is relatively low during the latest Carboniferous and Permian in comparison to the rest of the Palaeozoic and early Mesozoic (Fig. 3).

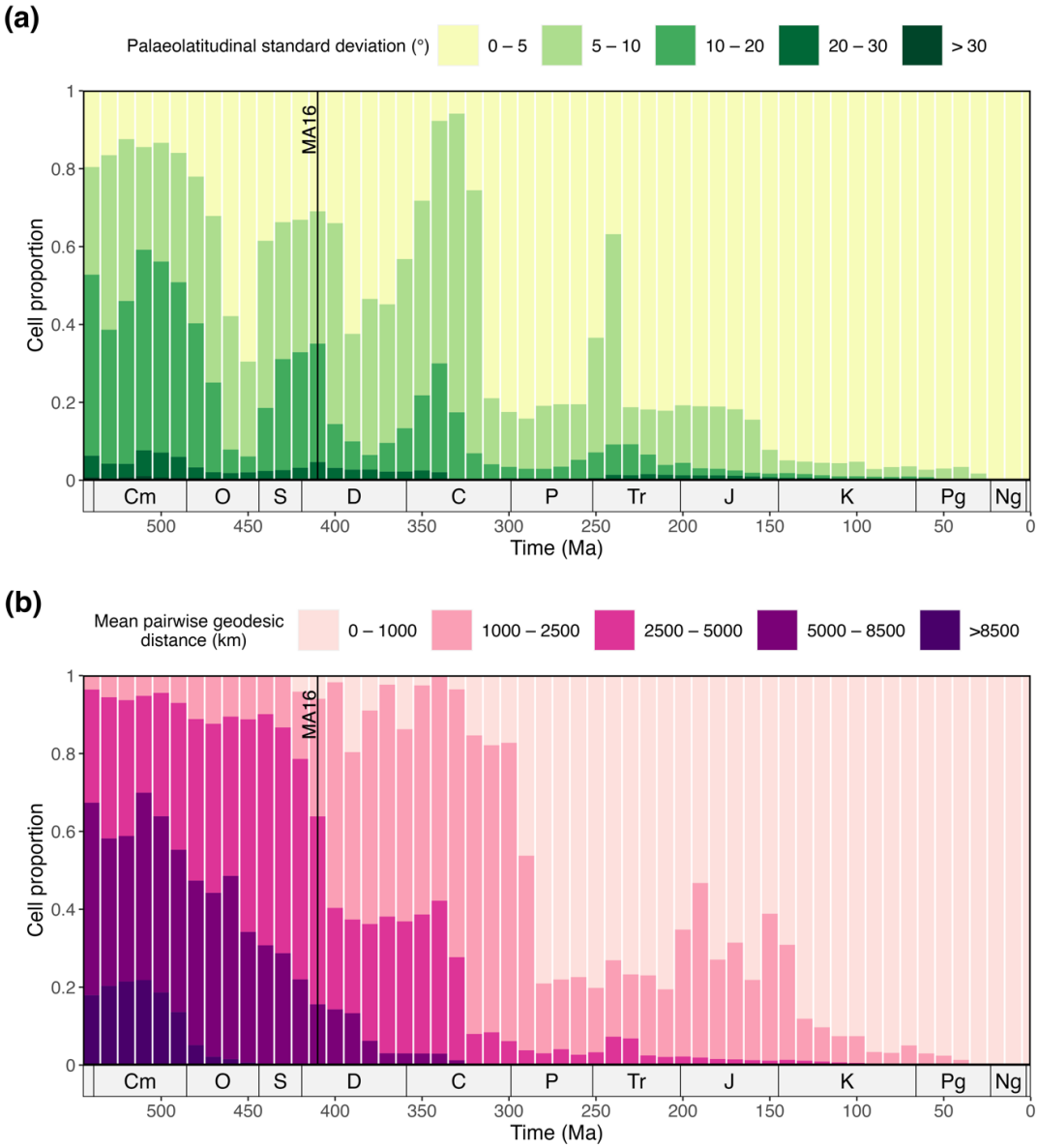

Figure 3: Phanerozoic trends in spatial discrepancies between Global Plate Models within 10 Myr time steps. Values are categorised and depicted as proportions of cells. (a) Palaeolatitudinal standard deviation between reconstructed palaeocoordinates for cell centroids. (b) Mean pairwise geodesic distance between reconstructed palaeocoordinates for cell centroids. The black line depicts the temporal limit (410 Ma) of the MA16 model (Matthews et al., 2016). The bar plots show increasing palaeogeographic uncertainty between models with age of reconstruction. Period abbreviations are as follows: Cambrian (Cm); Ordovician (O), Silurian (S), Devonian (D), Carboniferous (C), Permian (P),

Triassic (Tr), Jurassic (J), Cretaceous (K), Paleogene (Pg), and Neogene (Ng). The Quaternary is not depicted. The Geological Time Scale axis was added to the plot using the R package 'deeptime' ver. 1.0.1 (Gearty, 2023).

Our palaeolatitudinal SD and mean PGD results show palaeogeographic uncertainty is not evenly distributed in space (Fig. 4; Fig. S3). High palaeogeographic uncertainty is generally restricted to plate boundaries and active deformation zones during the Cenozoic and Mesozoic but extends to broader areas during the Palaeozoic (Fig. 4; Fig. S3; supplementary GIFs). For example, throughout the Cenozoic and Mesozoic, palaeogeographic reconstructions of South American cell centroids appear well constrained in comparison to those along the Eurasian-Indian and Eurasian-Arabian plate boundaries (Fig. 4; Fig. S3; supplementary GIFs).

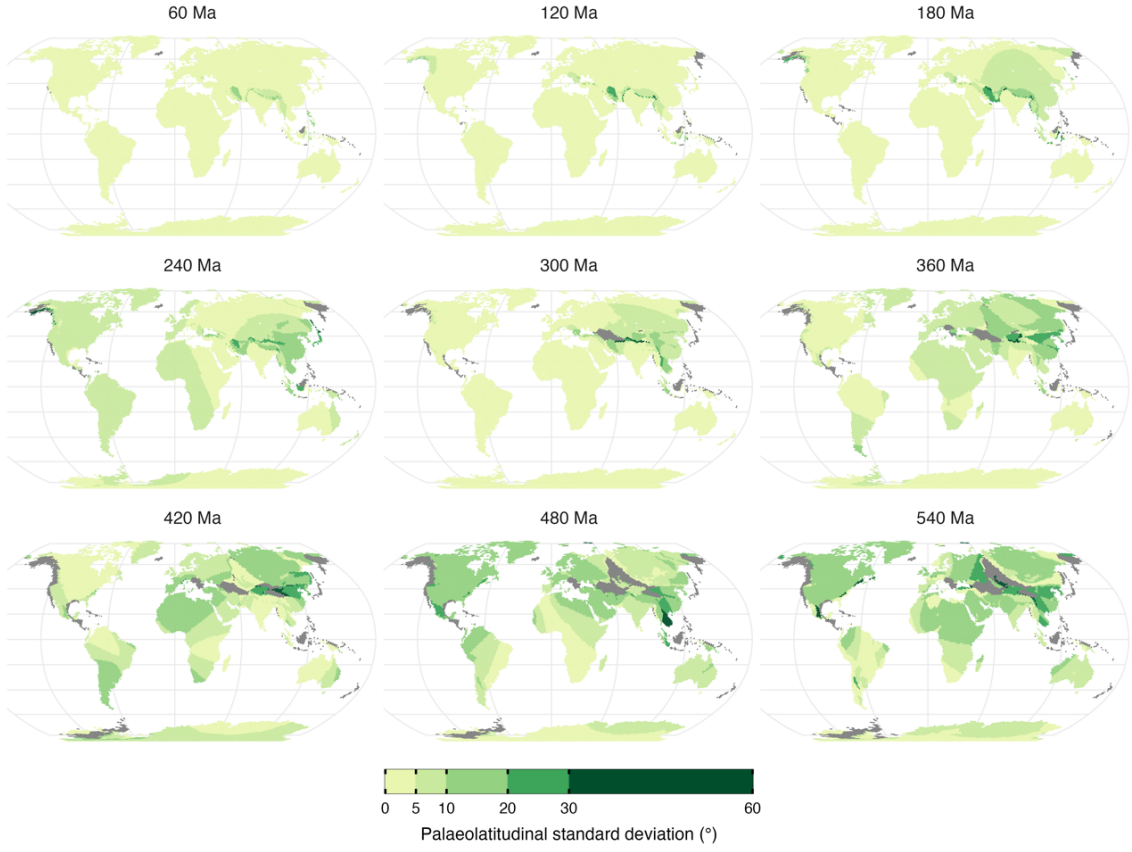

Figure 4: Categorised maps of the palaeolatitudinal standard deviation between reconstructed palaeocoordinates of cell centroids from Global Plate Models. Values are mapped onto a present-day

map with darker shades indicating greater palaeolatitudinal standard deviation between palaeocoordinates. Grey cells denote areas where palaeocoordinates could not be reconstructed at time of reconstruction for cell centroids by at least two models. Maps are presented in the Robinson projection (ESRI:54030).

Palaeoclimatic reconstructions

Our results suggest that reconstructions of the palaeolatitudinal extent of (sub-)tropical climatic conditions–based on terrestrial crocodylomorphs and coral reef occurrences–can vary by up to 12.3º latitude in crocodylomorphs and 24.1º in coral reefs, depending on GPM choice (Fig. 5). The average range between models along the 240 Myr time series is 7.7º for coral reefs and 6.5º for terrestrial crocodylomorphs (Fig. 5). However, despite these large observed differences, the direction of change (equatorward vs. poleward) in the extent of (sub-)tropical conditions is largely consistent between GPMs (Fig. 5). Both time series exhibit a significant positive correlation between age of reconstruction and the range in the extent of (sub-)tropical conditions from GPM estimates (Pearson's correlation test: $R = 0.43$; $P = 0.05$ for coral reefs and $R = 0.55$; $P = 0.005$ for crocodylomorphs). Comparisons of reconstructed palaeocoordinates for all occurrences further support an increase in palaeolatitudinal uncertainty with age (Fig. S5). For example, the average palaeolatitudinal range between the five GPMs for each occurrence–within each time bin–increases significantly with age (Pearson's correlation test: $R = 0.49$; $P < 0.001$ for coral reefs and $R = 0.33$; $P < 0.001$ for crocodylomorphs).

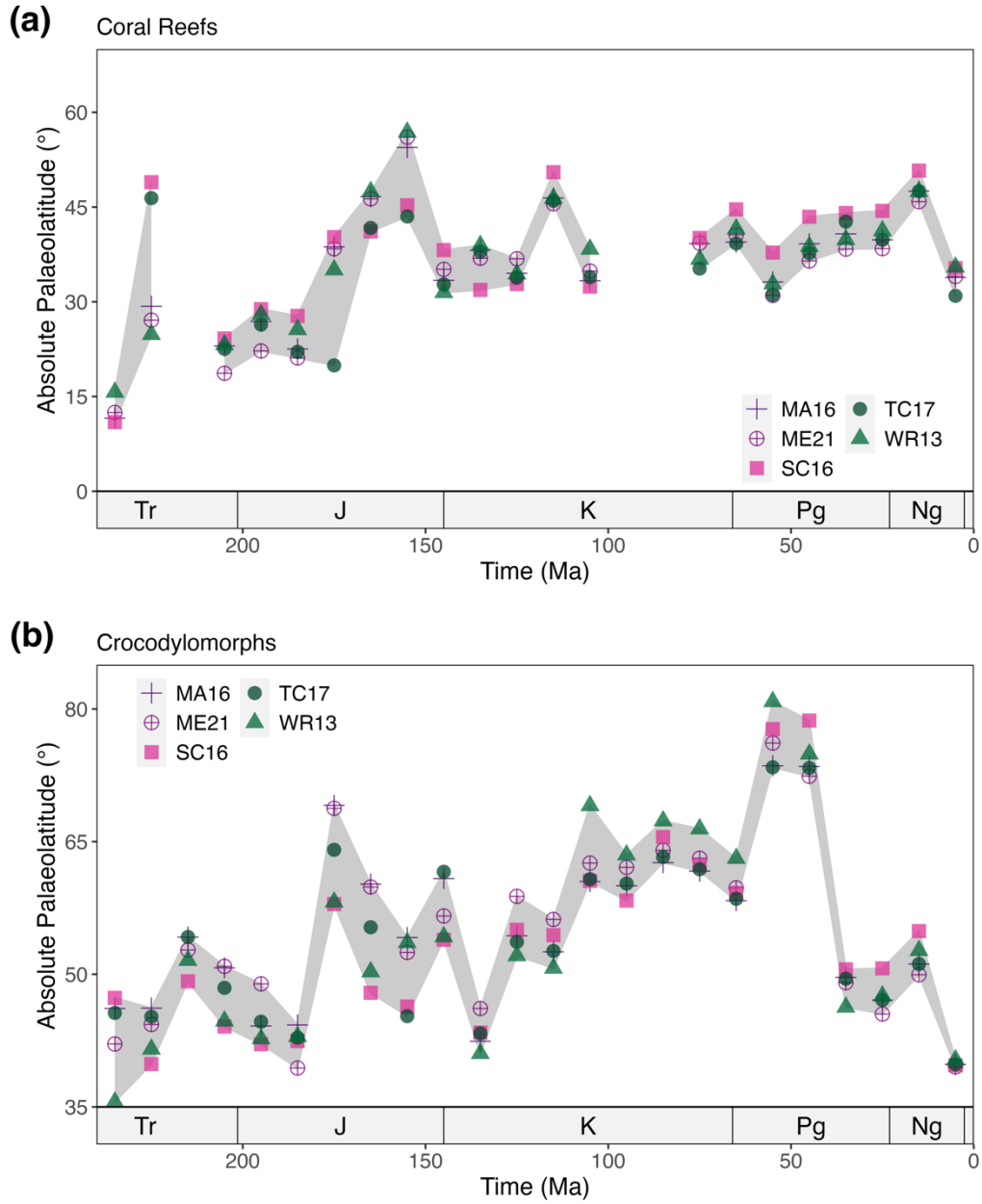

275

276 **Figure 5:** Palaeogeographic uncertainty in fossil-based reconstruction of the (sub-)tropics within 10
277 Myr time steps (0–240 Ma). For each time step, the maximum absolute reconstructed palaeolatitude of
278 coral reefs with a tropical affinity (a) and terrestrial crocodylomorphs (b) is depicted for each Global
279 Plate Model. The uncertainty of the palaeolatitudinal limit of subtropical reconstruction is depicted as
280 the range between the maximum absolute palaeolatitudes (grey ribbon), with an average uncertainty of
281 7.7° for coral reefs (a) and 6.5° for crocodylomorphs (b). Both time series exhibit a strong positive

correlation between age of reconstruction and palaeolatitudinal uncertainty (R = 0.43–0.55; $P \leq 0.05$). Global Plate Model abbreviations are the same as in Figure 1. The Geological Time Scale axis was added to the plot using the R package 'deeptime' ver. 1.0.1(Gearty, 2023).

Discussion

With age comes uncertainty

In this study, we quantified palaeogeographic reconstruction differences between five Global Plate Models (GPMs). Our results demonstrate that palaeogeographic uncertainty increases with age (Fig. 3) suggesting caution is required when reconstructing deep-time macroecological trends such as geographic range sizes (e.g. Antell et al., 2020), latitudinal biodiversity gradients (e.g. Powell, 2009; Zhang et al., 2022), and organisms' spatial response to global climatic change (e.g. Reddin et al., 2018). However, the issue of palaeogeographic uncertainty also has relevance for fields such as palaeoclimatology, where palaeotemperature proxies are used to reconstruct latitudinal temperature gradients (e.g. Zhang et al., 2019) and evaluate the performance of palaeoclimatic simulations (e.g. Lunt et al., 2021). Therefore, in the wake of additional methodological concerns that have been considered recently–e.g. spatial sampling bias in the geological record (e.g. Vilhena and Smith, 2013; Close et al., 2020; Jones and Eichenseer, 2021)–our work raises a new challenge for those working with fossil data in deep time. Following our results, we recommend that studies dealing with deep time palaeogeographic reconstructions should consider the robustness of their conclusions to GPM choice (e.g. Boddy et al., 2022), particularly for intervals older than ~300 Ma. Moreover, akin to phylogenies, we advocate that reconstructed coordinates should be treated as the model-based estimates they are, rather than empirical data.

Spatial clusters of palaeogeographic uncertainty

Our results show that palaeogeographic reconstruction discrepancies are not only uneven in time, but also in space. During the Cenozoic and Mesozoic, high palaeogeographic uncertainty is clustered around active plate boundaries and tectonically complex regions such as along the Eurasian-Indian,

Eurasian-Arabian, and North American-Juan de Fuca plate boundaries (Fig. 4; Fig. S3). The high uncertainty values found in these areas is a direct result of differential partitioning in GPMs with cell centroids assigned to different geometries, each with their own unique reconstruction history (Fig. S1). This finding suggests that additional caution is warranted when reconstructing the palaeogeographic distribution of fossil occurrences originating from areas close to plate boundaries or within tectonically complex regions. Hence, reconstructions of fossil occurrences from cratonic areas–stable interior portions of continents–ought to be more consistent between GPMs than reconstructions of fossil occurrences from continental margins or the edges of tectonic blocks. However, our results also suggest that there is an overarching trend of increasing uncertainty among GPMs throughout the Palaeozoic, even in cratonic areas. Rather than differences in the delineation of static polygons, this reflects differences in the modelled rotation histories as prescribed by the rotation files.

Pre-Jurassic palaeolongitudinal uncertainty

The direct reconstruction of palaeolongitude is challenging for most of Earth's history. While palaeomagnetic data can be used to constrain the relative palaeolatitudinal position of plates and continents, they cannot directly constrain palaeolongitude (Vérard, 2019). Hotspot tracks, which record the motion of a tectonic plate over a mantle plume, enable the determination of palaeolongitude (with respect to the base of the mantle), but owing to the incessant recycling of oceanic crust, well-resolved hotspot tracks are limited to the last ~130 Ma (Seton et al. 2023). Marine magnetic anomalies enable the determination of relative palaeolongitude back to the time of Pangaea breakup (~200 Ma), but they cannot constrain absolute palaeolongitude. Other attempts to constrain palaeolongitude in deeper time remain controversial (Torsvik et al., 2008b; Mitchell et al., 2012). This has broad implications for palaeobiological studies such as those reconstructing organisms' geographic range sizes in deep time (e.g. Kiessling and Aberhan, 2007). However, this will only be an issue in cases where occurrences span a relatively wide number of terranes. Nevertheless, one should also bear in mind that the palaeolatitudinal distribution of the continents can also vary significantly between GPMs particularly

in the Palaeozoic (Fig. S4), likely resulting from increasing sparsity of palaeomagnetic data over that period, as shown by Torsvik et al. (2012).

Reconstructing palaeoclimatic conditions

Fossil occurrences of climatically-sensitive organisms are routinely used to estimate the distribution of past climatic conditions (e.g. Frakes et al., 1992; Scotese et al., 2021; Burgener et al., 2023). Here–using five different GPMs–we estimated the palaeolatitudinal extent of (sub-)tropical climatic conditions for the last 240 Myr using fossil terrestrial crocodylomorphs and warm-water coral reefs (Fig. 5). Our findings support previous work in demonstrating that GPM choice can strongly influence reconstructions of palaeoclimatic conditions when based on geological data (e.g. Cao et al., 2019). Moreover, our results suggest that previous conclusions based on the use of one GPM might be worth revisiting (e.g. Markwick, 1998; Kiessling, 2001). Nevertheless, while large differences (~24.1º latitude) can be observed between GPMs in extreme cases, the direction of change (equatorward vs. poleward) is largely consistent between GPMs suggesting broad-scale relative patterns are constrained. Consequently–across temporal scales–the use of a single GPM can be useful for informing relative changes within a time series, but the magnitude of change relative to the present-day should be carefully considered.

Study limitations

We quantified Phanerozoic (540–0 Ma) palaeogeographic uncertainty between five GPMs using a global hexagonal grid (~100 km spacings). While the use of additional models such as the commonly applied Getech plate model would be desirable to further quantify palaeogeographic uncertainty (e.g. Chiarenza et al., 2019; Saupe et al., 2019), not all GPMs are open access and broadly available to the community. Despite this, the use of additional models is unlikely to change the general trends observed in this study which are primarily driven by limited data availability (e.g. palaeomagnetic data and constraints on palaeolongitude) and geological interpretation (e.g. tectonic boundaries). Furthermore, the spatial resolution of our study (~100 km spacings) may influence our results in the identification of

areas of high palaeogeographic uncertainty. For example, along geological boundaries, a finer-scale grid might further constrain the areal extent of these areas. Nevertheless, our results provide a first-order advisory note for those working with spatial data and advocates for the quantification of palaeogeographic uncertainty for individual datasets.

Conclusion

In conclusion, our study demonstrates that differences in palaeogeographic reconstruction increase with age. Consequently, an increasing level of caution is warranted when reconstructing fossil assemblages from older intervals, particularly for intervals older than ~300 Ma. Nevertheless, consideration is also required–even for younger intervals–for fossil occurrences originating from tectonically complex regions where the definition of tectonic boundaries lack consensus between Global Plate Models. Our study also demonstrates the impact Global Plate Model choice can have on broader conclusions such as reconstructions of palaeoclimatic conditions based on fossil occurrence data. Therefore, we endorse that studies dependent on deep-time palaeogeographic reconstructions should only use models based on a palaeomagnetic reference frame to reconstruct fossil palaeocoordinates, test the sensitivity of their conclusions to Global Plate Model choice, and quantify the palaeogeographic uncertainty associated with their data.

Acknowledgements

We are grateful for the efforts of all those who have contributed to collecting the fossil data used in this study and entering them into the Paleobiology Database and the PaleoReefs Database. L.B. was funded by the École Normale Supérieure de Lyon, France. L.A.J. and S.V. were funded by the European Research Council under the European Union's Horizon 2020 research and innovation program (grant agreement 947921) as part of the MAPAS project. L.A.J. was also supported by a Juan de la Cierva-formación 2021 fellowship (FJC2021-046695-I) funded by MCIN/AEI/10.13039/501100011033 and the European Union NextGenerationEU/PRTR. SZ was supported by Australian Research Council grant DE210100084. (py)GPlates development is funded by the AuScope National Collaborative

Research Infrastructure System (NCRIS) program. This is Palaeobiology Database publication no XXX.

Authors' contributions

LAJ and SV conceived the project. All authors contributed to developing the project. LB, LAJ and MD wrote the code, conducted the analyses, and produced the figures. All authors contributed to writing the manuscript.

Data availability

The data generated in this study have been included within the paper, its supplementary material, and dedicated GitHub repository (https://github.com/Buffan3369/rotation_sensitivity).

Code availability

Generation of the reconstruction grids and palaeocoordinates for fossil occurrence data were generated via pygplates run in python version 3.9.7. All data analyses were conducted in R version 4.2.2. The workflow is available both as R scripts and Jupyter notebooks on GitHub (accessible via: https://github.com/Buffan3369/rotation_sensitivity).

References

Allen, B.J., Wignall, P.B., Hill, D.J., Saupe, E.E., and Dunhill, A.M., 2020, The latitudinal diversity gradient of tetrapods across the Permo-Triassic mass extinction and recovery interval: Proceedings of the Royal Society B: Biological Sciences, v. 287, doi:10.1098/rspb.2020.1125.

Alroy, J., 2014, Accurate and precise estimates of origination and extinction rates: Paleobiology, v. 40, p. 374–397, doi:10.1666/13036.

Antell, G.S., Kiessling, W., Aberhan, M., and Saupe, E.E., 2020, Marine Biodiversity and Geographic Distributions Are Independent on Large Scales: Current Biology, v. 30, p. 115- 121.e5, doi:10.1016/j.cub.2019.10.065.

Boddy, C.E., Mitchell, E.G., Merdith, A., and Liu, A.G., 2022, Palaeolatitudinal distribution of the Ediacaran macrobiota: Journal of the Geological Society, v. 179, p. jgs2021- 030, doi:10.1144/jgs2021-030.

Boyden, J.A., Müller, R.D., Gurnis, M., Torsvik, T.H., Clark, J.A., Turner, M., Ivey-Law, H., Watson, R.J., and Cannon, J.S., 2011, Next-generation plate-tectonic reconstructions using GPlates, *in*

410 Geoinformatics: Cyberinfrastructure for the Solid Earth Sciences, Cambridge, Cambridge
411 University Press, p. 95–113.

412 Brocklehurst, N., Day, M.O., Rubidge, B.S., and Fröbisch, J., 2017, Olson's extinction and the
413 latitudinal biodiversity gradient of tetrapods in the Permian: Proceedings of the Royal Society
414 B: Biological Sciences, v. 284, p. 1–8.

415 Burgener, L., Hyland, E., Reich, B.J., and Scotese, C., 2023, Cretaceous climates: Mapping paleo-
416 Köppen climatic zones using a Bayesian statistical analysis of lithologic, paleontologic, and
417 geochemical proxies: Palaeogeography, Palaeoclimatology, Palaeoecology, v. 613, p. 111373,
418 doi:10.1016/j.palaeo.2022.111373.

419 Cao, W., Williams, S., Flament, N., Zahirovic, S., Scotese, C., and Müller, R.D., 2019, Palaeolatitudinal
420 distribution of lithologic indicators of climate in a palaeogeographic framework: Geological
421 Magazine, v. 156, p. 331–354, doi:10.1017/S0016756818000110.

422 Chiarenza, A.A., Mannion, P.D., Lunt, D.J., Farnsworth, A., Jones, L.A., Kelland, S.-J., and Allison,
423 P.A., 2019, Ecological niche modelling does not support climatically-driven dinosaur diversity
424 decline before the Cretaceous/Paleogene mass extinction: Nature Communications, v. 10, p. 1–
425 14, doi:10.1038/s41467-019-08997-2.

426 Close, R.A., Benson, R.B.J., Saupe, E.E., Clapham, M.E., and Butler, R.J., 2020, The spatial structure
427 of Phanerozoic marine animal diversity: Science, v. 368, p. 420–424,
428 doi:10.1126/science.aay8309.

429 Domeier, M., 2016, A plate tectonic scenario for the Iapetus and Rheic oceans: Gondwana Research, v.
430 36, p. 275–295, doi:10.1016/j.gr.2015.08.003.

431 Domeier, M., 2018, Early Paleozoic tectonics of Asia: Towards a full-plate model: Geoscience
432 Frontiers, v. 9, p. 789–862, doi:10.1016/j.gsf.2017.11.012.

433 Domeier, M., and Torsvik, T.H., 2019, Full-plate modelling in pre-Jurassic time: Geological Magazine,
434 v. 156, p. 261–280.

435 Domeier, M., and Torsvik, T.H., 2014, Plate tectonics in the late Paleozoic: Geoscience Frontiers, v. 5,
436 p. 303–350, doi:10.1016/j.gsf.2014.01.002.

437 Dunne, E.M., Farnsworth, A., Greene, S.E., Lunt, D.J., and Butler, R.J., 2020, Climatic drivers of
438 latitudinal variation in Late Triassic tetrapod diversity: Palaeontology, v. 64, p. 101–117,
439 doi:https://doi.org/10.1111/pala.12514.

440 Frakes, L.A., Francis, J.E., and Syktus, J.I., 1992, Climate Modes of the Phanerozoic: Cambridge,
441 Cambridge University Press, doi:10.1017/CBO9780511628948.

442 Gearty, W., 2023, deeptime: Plotting Tools for Anyone Working in Deep Time. R package version
443 1.0.1.:, https://CRAN.R-project.org/package=deeptime.

444 Golonka, J., 2007, Late Triassic and Early Jurassic palaeogeography of the world: Palaeogeography,
445 Palaeoclimatology, Palaeoecology, v. 244, p. 297–307.

446 Golonka, J.R., Ross, M.I., and Scotese, C.R., 1994, Phanerozoic paleogeographic and paleoclimatic

447 modeling maps: Pangea: Global Environments and Resources, v. 17, p. 1–47.

448 Gurnis, M., Yang, T., Cannon, J., Turner, M., Williams, S., Flament, N., and Müller, R.D., 2018, Global
449 tectonic reconstructions with continuously deforming and evolving rigid plates: Computers &
450 Geosciences, v. 116, p. 32–41, doi:10.1016/j.cageo.2018.04.007.

451 Hijmans, R.J., Karney (GeographicLib), C., Williams, E., and Vennes, C., 2021, geosphere: Spherical
452 Trigonometry:, https://CRAN.R-project.org/package=geosphere (accessed February 2022).

453 Jones, L.A., and Eichenseer, K., 2021, Uneven spatial sampling distorts reconstructions of Phanerozoic
454 seawater temperature: Geology, doi:10.1130/G49132.1.

455 Jones, L.A., Mannion, P.D., Farnsworth, A., Bragg, F., and Lunt, D.J., 2022, Climatic and tectonic
456 drivers shaped the tropical distribution of coral reefs: Nature Communications, v. 13, p. 3120,
457 doi:10.1038/s41467-022-30793-8.

458 Kiessling, W., 2001, Paleoclimatic significance of Phanerozoic reefs: Geology, v. 29, p. 751–754,
459 doi:10.1130/0091-7613(2001)029<0751:PSOPR>2.0.CO;2.

460 Kiessling, W., and Aberhan, M., 2007, Geographical distribution and extinction risk: lessons from
461 Triassic–Jurassic marine benthic organisms: Journal of Biogeography, v. 34, p. 1473–1489,
462 doi:10.1111/j.1365-2699.2007.01709.x.

463 Kiessling, W., and Krause, M.C., 2022, PARED - An online database of Phanerozoic reefs: PARED -
464 An online database of Phanerozoic reefs, https://www.paleo-reefs.pal.uni-erlangen.de
465 (accessed October 2021).

466 Lunt, D.J. et al., 2021, DeepMIP: model intercomparison of early Eocene climatic optimum (EECO)
467 large-scale climate features and comparison with proxy data: Climate of the Past, v. 17, p. 203–
468 227, doi:10.5194/cp-17-203-2021.

469 Lunt, D.J., Farnsworth, A., Loptson, C., Foster, G.L., Markwick, P., O'Brien, C.L., Pancost, R.D.,
470 Robinson, S.A., and Wrobel, N., 2016, Palaeogeographic controls on climate and proxy
471 interpretation: Climate of the Past, v. 12, p. 1181–1198, doi:10.5194/cp-12-1181-2016.

472 Mannion, P.D., Benson, R.B.J., Carrano, M.T., Tennant, J.P., Judd, J., and Butler, R.J., 2015, Climate
473 constrains the evolutionary history and biodiversity of crocodylians: Nature Communications,
474 v. 6, p. 8438, doi:10.1038/ncomms9438.

475 Mannion, P.D., Upchurch, P., Benson, R.B.J., and Goswami, A., 2014, The latitudinal biodiversity
476 gradient through deep time: Trends in Ecology & Evolution, v. 29, p. 42–50,
477 doi:10.1016/j.tree.2013.09.012.

478 Markwick, P.J., 1998, Crocodilian diversity in space and time: the role of climate in paleoecology and
479 its implication for understanding K/T extinctions: Paleobiology, v. 24, p. 470–497,
480 doi:10.1017/S009483730002011X.

481 Markwick, P.J., 2019, Palaeogeography in exploration: Geological Magazine, v. 156, p. 366–407.

482 Markwick, P.J., 2007, The palaeogeographic and palaeoclimatic significance of climate proxies for
483 data-model comparisons, *in* Williams, M., Haywood, A.M., Gregory, F.J., and Schmidt, D.N.

484 eds., Deep-Time Perspectives on Climate Change: Marrying the Signal from Computer Models
485 and Biological Proxies, The Geological Society of London on behalf of The
486 Micropalaeontological Society, p. 251–312, doi:10.1144/TMS002.13.

487 Matthews, K.J., Maloney, K.T., Zahirovic, S., Williams, S.E., Seton, M., and Müller, R.D., 2016,
488 Global plate boundary evolution and kinematics since the late Paleozoic: Global and Planetary
489 Change, v. 146, p. 226–250, doi:10.1016/j.gloplacha.2016.10.002.

490 McKenzie, D.P., and Parker, R.L., 1967, The North Pacific: an example of tectonics on a sphere: Nature,
491 v. 216, p. 1276–1280.

492 Merdith, A.S. et al., 2017, A full-plate global reconstruction of the Neoproterozoic: Gondwana
493 Research, v. 50, p. 84–134, doi:10.1016/j.gr.2017.04.001.

494 Merdith, A.S. et al., 2021, Extending full-plate tectonic models into deep time: Linking the
495 Neoproterozoic and the Phanerozoic: Earth-Science Reviews, v. 214, p. 103477,
496 doi:10.1016/j.earscirev.2020.103477.

497 Meseguer, A.S., and Condamine, F.L., 2020, Ancient tropical extinctions at high latitudes contributed
498 to the latitudinal diversity gradient: Evolution, p. 1–22, doi:10.1111/evo.13967.

499 Mitchell, R.N., Kilian, T.M., and Evans, D.A.D., 2012, Supercontinent cycles and the calculation of
500 absolute palaeolongitude in deep time: Nature, v. 482, p. 208–211, doi:10.1038/nature10800.

501 Morgan, W.J., 1968, Rises, trenches, great faults, and crustal blocks: Journal of Geophysical Research,
502 v. 73, p. 1959–1982.

503 Müller, R.D. et al., 2019, A Global Plate Model Including Lithospheric Deformation Along Major Rifts
504 and Orogens Since the Triassic: Tectonics, v. 38, p. 1884–1907, doi:10.1029/2018TC005462.

505 Müller, R.D. et al., 2016, Ocean Basin Evolution and Global-Scale Plate Reorganization Events Since
506 Pangea Breakup: Annual Review of Earth and Planetary Sciences, v. 44, p. 107–138,
507 doi:10.1146/annurev-earth-060115-012211.

508 Müller, R.D., Cannon, J., Qin, X., Watson, R.J., Gurnis, M., Williams, S., Pfaffelmoser, T., Seton, M.,
509 Russell, S.H.J., and Zahirovic, S., 2018, GPlates: Building a Virtual Earth Through Deep Time:
510 Geochemistry, Geophysics, Geosystems, v. 19, p. 2243–2261,
511 doi:https://doi.org/10.1029/2018GC007584.

512 Müller, R.D., Royer, J.-Y., and Lawver, L.A., 1993, Revised plate motions relative to the hotspots from
513 combined Atlantic and Indian Ocean hotspot tracks: Geology, v. 21, p. 275–278,
514 doi:10.1130/0091-7613(1993)021<0275:RPMRTT>2.3.CO;2.

515 Powell, M.G., 2009, The Latitudinal Diversity Gradient of Brachiopods over the Past 530 Million
516 Years: The Journal of Geology, v. 117, p. 585–594, doi:10.1086/605777.

517 Powell, M.G., Moore, B.R., and Smith, T.J., 2015, Origination, extinction, invasion, and extirpation
518 components of the brachiopod latitudinal biodiversity gradient through the Phanerozoic Eon:
519 Paleobiology, v. 41, p. 330–341.

520 Reddin, C.J., Kocsis, Á.T., and Kiessling, W., 2018, Marine invertebrate migrations trace climate

change over 450 million years: Global Ecology and Biogeography, v. 27, p. 704–713, doi:10.1111/geb.12732.

Saupe, E.E., Farnsworth, A., Lunt, D.J., Sagoo, N., Pham, K.V., and Field, D.J., 2019, Climatic shifts drove major contractions in avian latitudinal distributions throughout the Cenozoic: Proceedings of the National Academy of Sciences, v. 116, p. 12895–12900, doi:10.1073/pnas.1903866116.

Scotese, C., 2004, A Continental Drift Flipbook: Journal of Geology, v. 112, p. 729–741, doi:10.1086/424867.

Scotese, C.R., 2016, Tutorial: PALEOMAP paleoAtlas for GPlates and the paleoData plotter program: PALEOMAP Project, Technical Report,.

Scotese, C.R., and Elling, R., 2017, Plate Tectonic Evolution during the last 1.3 billion years: The Movie., *in* Burlington House, London, The Geological Society of London, p. 16–17.

Scotese, C.R., Gahagan, L.M., and Larson, R.L., 1988, Plate tectonic reconstructions of the Cretaceous and Cenozoic ocean basins: Tectonophysics, v. 155, p. 27–48, doi:10.1016/0040-1951(88)90259-4.

Scotese, C.R., Song, H., Mills, B.J.W., and van der Meer, D.G., 2021, Phanerozoic paleotemperatures: The earth's changing climate during the last 540 million years: Earth-Science Reviews, v. 215, p. 103503, doi:10.1016/j.earscirev.2021.103503.

Scotese, C., and Wright, N.M., 2018, PALEOMAP Paleodigital Elevation Models (PaleoDEMs) for the Phanerozoic PALEOMAP Project:, https://www.earthbyte.org/paleodem-resource-scotese-and-wright-2018/.

Seton, M. et al., 2012, Global continental and ocean basin reconstructions since 200 Ma: Earth-Science Reviews, v. 113, p. 212–270, doi:10.1016/j.earscirev.2012.03.002.

Seton, M., Williams, S.E., Domeier, M., Collins, A.S., and Sigloch, K., 2023, Deconstructing plate tectonic reconstructions: Nature Reviews Earth & Environment, p. 1–20, doi:10.1038/s43017-022-00384-8.

Song, H., Huang, S., Jia, E., Dai, X., Wignall, P.B., and Dunhill, A.M., 2020, Flat latitudinal diversity gradient caused by the Permian–Triassic mass extinction: Proceedings of the National Academy of Sciences, p. 1–6, doi:10.1073/pnas.1918953117.

Spano, C.A., Hernández, C.E., and Rivadeneira, M.M., 2016, Evolutionary dispersal drives the latitudinal diversity gradient of stony corals: Ecography, v. 39, p. 836–843, doi:10.1111/ecog.01855.

Torsvik, T.H. et al., 2012, Phanerozoic polar wander, palaeogeography and dynamics: Earth-Science Reviews, v. 114, p. 325–368, doi:10.1016/j.earscirev.2012.06.007.

Torsvik, T.H., and Cocks, L.R.M., 2017, Earth history and palaeogeography:

Torsvik, T.H., Müller, R.D., Van der Voo, R., Steinberger, B., and Gaina, C., 2008a, Global plate motion frames: Toward a unified model: Reviews of Geophysics, v. 46,

558 doi:10.1029/2007RG000227.

559 Torsvik, T.H., Steinberger, B., Cocks, L.R.M., and Burke, K., 2008b, Longitude: Linking Earth's
560 ancient surface to its deep interior: Earth and Planetary Science Letters, v. 276, p. 273–282,
561 doi:10.1016/j.epsl.2008.09.026.

562 Torsvik, T.H., and Van der Voo, R., 2002, Refining Gondwana and Pangea palaeogeography: estimates
563 of Phanerozoic non-dipole (octupole) fields: Geophysical Journal International, v. 151, p. 771–
564 794, doi:10.1046/j.1365-246X.2002.01799.x.

565 Uber, 2023, h3-py: Uber's H3 Hexagonal Hierarchical Geospatial Indexing System in Python:,
566 https://github.com/uber/h3-py.

567 Vérard, C., 2019, Plate tectonic modelling: review and perspectives: Geological Magazine, v. 156, p.
568 208–241, doi:10.1017/S0016756817001030.

569 Vilhena, D.A., and Smith, A.B., 2013, Spatial Bias in the Marine Fossil Record: PLoS ONE, v. 8, p. 1–
570 7, doi:10.1371/journal.pone.0074470.

571 Williams, S., Cannon, J., Qin, X., and Müller, D., 2017, PyGPlates - a GPlates Python library for data
572 analysis through space and deep geological time: , p. 8556.

573 Wright, N., Zahirovic, S., Müller, R.D., and Seton, M., 2013, Towards community-driven
574 paleogeographic reconstructions: integrating open-access paleogeographic and paleobiology
575 data with plate tectonics: Biogeosciences, v. 10, p. 1529–1541, doi:10.5194/bg-10-1529-2013.

576 Young, A., Flament, N., Maloney, K., Williams, S., Matthews, K., Zahirovic, S., and Müller, R.D.,
577 2019, Global kinematics of tectonic plates and subduction zones since the late Paleozoic Era:
578 Geoscience Frontiers, v. 10, p. 989–1013, doi:10.1016/j.gsf.2018.05.011.

579 Zhang, L., Hay, W.W., Wang, C., and Gu, X., 2019, The evolution of latitudinal temperature gradients
580 from the latest Cretaceous through the Present: Earth-Science Reviews, v. 189, p. 147–158,
581 doi:10.1016/j.earscirev.2019.01.025.

582 Zhang, S.-H., Shen, S.-Z., and Erwin, D.H., 2022, Latitudinal diversity gradient dynamics during
583 Carboniferous to Triassic icehouse and greenhouse climates: Geology, v. 50, p. 1166–1171,
584 doi:10.1130/G50110.1.

585